Hybrid approach predicts a lower binding energy for benzene on water ice

Clark, V.H.J.; Benoit, D.M.; Van de Sande, M.L.; Walsh, C.

Monthly Notices of the ROYAL ASTRONOMICAL SOCIETY

MNRAS **532,** 3499–3508 (2024)
Advance Access publication 2024 June 28

https://doi.org/10.1093/mnras/stae1605

Hybrid approach predicts a lower binding energy for benzene on water ice

Victoria H. J. Clark [1], David M. Benoit [2★], Marie Van de Sande [3,4★] and Catherine Walsh [3★]

[1] *Department of Physics and Astronomy, University College London, London WC1E 6BT, UK*
[2] *E.A. Milne Centre for Astrophysics, University of Hull, Hull HU6 7RX, UK*
[3] *School of Physics and Astronomy, University of Leeds, Leeds LS2 9JT, UK*
[4] *Leiden Observatory, Leiden University, PO Box 9513, NL-2300 RA Leiden, the Netherlands*

Accepted 2024 June 18. Received 2024 June 13; in original form 2023 November 30

ABSTRACT

In this paper, we provide a highly accurate value for the binding energy of benzene to proton-ordered crystalline water ice (XIh), as a model for interstellar ices. We compare our computed value to the latest experimental data available from temperature-programmed desorption experiments and find that our binding energy value agrees well with data obtained from binding to either crystalline or amorphous ice. Importantly, our new value is lower than that used in most astrochemical networks by about nearly half its value. We explore the impact of this revised binding energy value for both an asymptotic giant branch (AGB) outflow and a protoplanetary disc. We find that the lower value of the binding energy predicted here compared with values used in the literature (4050 K versus 7587 K) leads to less depletion of gas-phase benzene in an AGB outflow, and leads to a shift outwards in the benzene snowline in the mid-plane of a protoplanetary disc. Using this new value, the AGB model predicts lower abundances of benzene in the solid phase throughout the outflow. The disc model also predicts a larger reservoir of gas-phase benzene in the inner disc, which is consistent with the recent detections of benzene for the first time in protoplanetary discs with *JWST*.

Key words: astrochemistry – molecular data – ISM: molecules.

1 INTRODUCTION

Cernicharo et al. (2001) first detected benzene in a planetary nebula (CRL618) at the start of this century. Although difficult to observe, benzene has also since been detected in a number of other astronomical environments such as post-asymptotic giant branch (post-AGB) objects in the Small Magellanic Cloud (Kraemer et al. 2006), circumstellar envelopes of carbon-rich evolved stars (Malek, Cami & Bernard-Salas 2012), and the comae of comets and asteroids (Schuhmann et al. 2019). Closer to Earth, benzene has also been detected in the atmosphere of Saturn (Koskinen et al. 2016) and in Titan's atmosphere (Waite et al. 2007), and has also long been identified as a component of meteoritic chondrites (Delsemme 1975).

Thanks to high-sensitivity observations with *JWST*, benzene has now also been detected for the first time in the inner regions of two protoplanetary discs around low-mass stars, with a high column density of 28 and 68 per cent that of C_2H_2, respectively (Tabone et al. 2023; Arabhavi et al. 2024). These new detections of abundant benzene in protoplanetary discs have prompted renewed interest in this molecule, well motivating the need for the quantification of fundamental data pertinent to benzene chemistry in such environments, such as its binding energy to astrophysical ices and corresponding spectral features in the solid phase. Indeed, a number of recent studies (Ferrero et al. 2020; Bovolenta et al. 2022; Tinacci et al. 2022) and reviews (Zamirri et al. 2019) have highlighted the importance of accurate binding energies for astrochemical simulations of smaller adsorbed molecules. Furthermore, a suitable radio proxy for benzene has been identified as cyanobenzene (Cooke et al. 2020), due to its rapid reaction with CN even at low cold interstellar medium temperatures. Indeed, cyanobenzene was first detected in the Taurus Molecular Cloud (TMC-1) by McGuire et al. (2018) and has now also been further confirmed in pre-stellar sources (Burkhardt et al. 2021).

Benzene is also becoming a more popular component of kinetic reaction networks in dust grain models, since Jones et al. (2011) showed that it could be formed through a barrierless reaction. However, an accurate binding energy data is key to providing a realistic account of the residence time of benzene on ice and describing the desorption process. Currently, the most popular value of benzene–ice binding energy used in those models (e.g. Rate12; McElroy et al. 2013) originates from an additive estimation by Garrod & Herbst (2006). In this study, we suggest a new value obtained through high-level ab initio modelling of the binding of benzene to an ordered ice surface. We also compare our data to the latest temperature-programmed desorption (TPD) experimental values (Thrower et al. 2009; Stubbing 2019).

We recently showed (Clark & Benoit 2019) the feasibility of a molecular arrangement where benzene acts as a hydrogen-bond acceptor to the dangling O–H bonds of the ice surface. Indeed,

★ E-mail: d.benoit@hull.ac.uk (DMB); mvdsande@strw.leidenuniv.nl (MVdS); c.walsh1@leeds.ac.uk (CW)

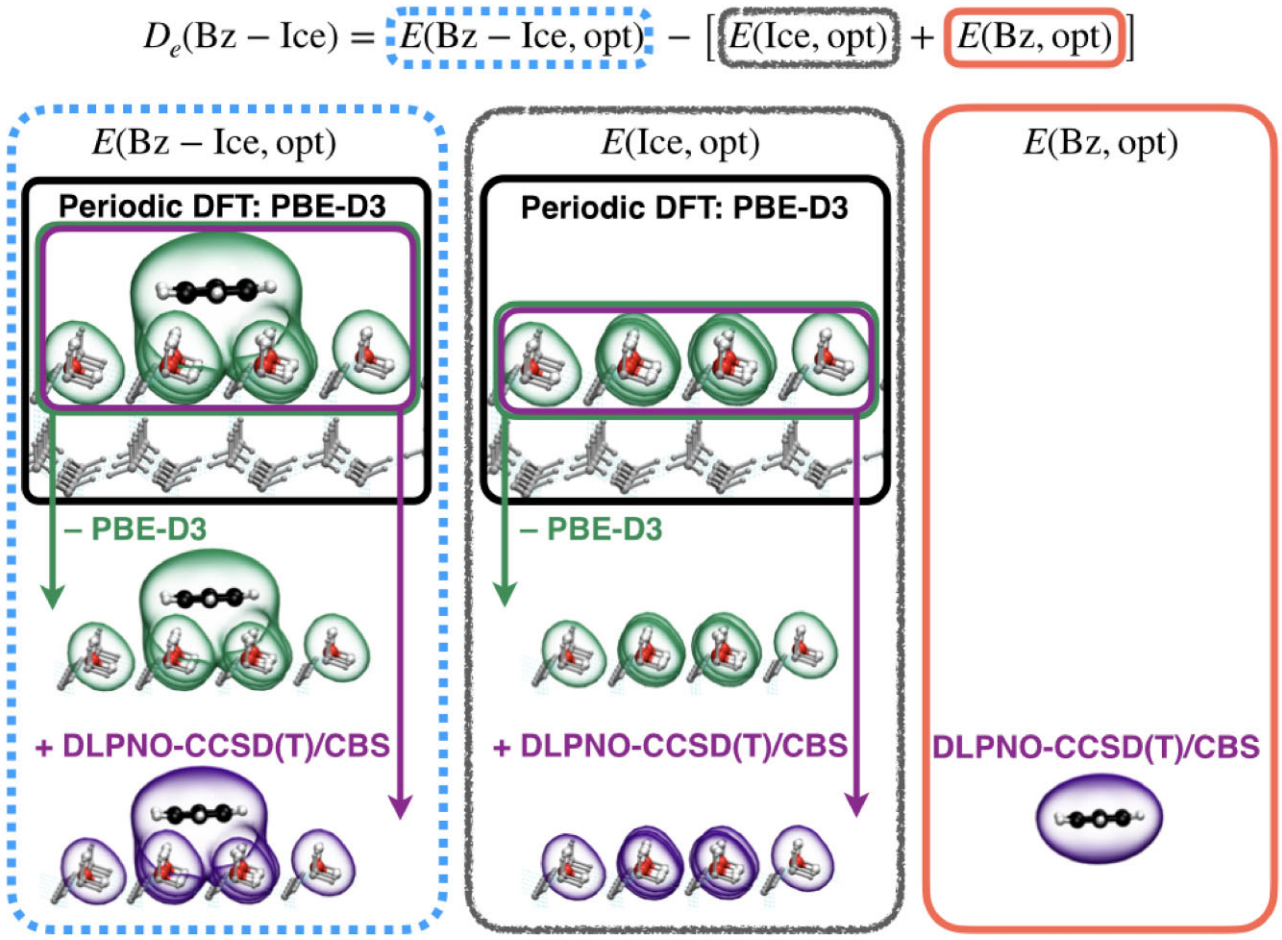

Figure 1. Representation of the ONIOM approach used to compute the adsorption energy of benzene on an ice surface model. Each component of the energy expression at the top is decomposed into up to three calculations: two periodic DFT calculations (full system and model) and one DLPNO-CCSD(T) calculation (model). The full system optimized at the PBE-D3/MOLOPT-TZV2P is shown at the top of each panel. Note that the benzene component is simply computed directly at the DLPNO-CCSD(T)/CBS level using an optimized PBE-D3/MOLOPT-TZV2P geometry. PBE-D3 calculations are indicated using a green colour and the DLPNO-CCSD(T) calculations using a purple colour.

such π–hydrogen bonding was suggested already by Silva & Devlin (1994) and has also been identified for benzene–water clusters (Engdahl & Nelander 1985; Gotch & Zwier 1992; Suzuki et al. 1992; Benoit, Chavagnac & Clary 1998). We also explored the influence of such a binding mode on the vibrational spectrum of benzene (Clark & Benoit 2021) and showed how our ordered ice surface model was able to rationalize the laboratory-based infrared observations. This study builds on these findings and has two aims: first, we use our surface model to provide a new reliable upper bound (i.e. largest) value for the binding energy of benzene on a water ice surface. Secondly, we explore the effects of using this revised binding energy for two astrophysically relevant scenarios, namely AGB outflows and protoplanetary disc models.

Our study is organized as follows: in Section 2, we describe a hybrid approach to compute the binding energy of benzene adsorbed on a ferroelectric proton-ordered hexagonal crystalline water ice (XIh) surface and compare our values to the latest available experimental data. This ferroelectric surface provides us with a model of the most favourable (i.e. highest possible) binding energy for an adsorbed molecule on ice. Our computational details are outlined in Section 3. In Section 4, we present our new binding energy value for this system (along with derived data) and computational results exploring the implications of a weaker binding energy for astrophysical situations. Our conclusions can then be found in Section 5.

2 SURFACE BINDING ENERGY MODEL

We use an ordered model for crystalline interstellar ice, built from the basal plane surface of ferroelectric water ice XIh, as described in our earlier work (Clark & Benoit 2021). The binding energies for the benzene to the ice surface are computed using a technique that mixes periodic density functional theory (DFT) with coupled-cluster singles and doubles with perturbative triples [CCSD(T)] calculations. The scheme, referred to later on as DFT/CCSD(T), is a version of the 'our own *n*-layered integrated molecular orbital and molecular mechanics' (ONIOM) approach developed by Morokuma and collaborators (see Dapprich et al. 1999). We use the optimized geometry of benzene molecule adsorbed on the *topmost* surface layer of the ice XIh obtained in Clark & Benoit (2021) (details in Section 3). The system is then divided into multiple parts as shown in Fig. 1.

Following the framework of the ONIOM approach, each component of the binding energy is systematically improved using an efficient implementation of the domain-based local-pair natural or-

bital CCSD(T) theory, DLPNO-CCSD(T), extrapolated to complete basis set (CBS) limit (see Section 3 for details).

We define the binding energy of a benzene molecule as a negative quantity,

$$D_{e(\mathrm{Bz-Ice})} = E_{(\mathrm{Bz-Ice,opt})} - \left[E_{(\mathrm{Ice,opt})} + E_{(\mathrm{Bz,opt})}\right], \quad (1)$$

where the opt label refers to an optimization using dispersion corrected Perdew, Burke, and Ernzerhof functional along with a molecular optimised basis set (PBE-D3/MOLOPT-TZV2P level of theory), $E_{(\mathrm{Bz-Ice,opt})}$ refers to the bound benzene on ice, $E_{(\mathrm{Ice,opt})}$ refers to the pure ice surface, and $E_{(\mathrm{Bz,opt})}$ refers to the gaseous benzene structure. Each component on the right of equation (1) is then computed using a two-level ONIOM approach such that

$$E_{(\mathrm{Bz-Ice,opt})} = E^{\mathrm{low}}_{(\mathrm{Bz-Ice,opt})} - \left[E^{\mathrm{low}}_{(\mathrm{model})} + E^{\mathrm{high}}_{(\mathrm{model})}\right], \quad (2)$$

$$E_{(\mathrm{Ice,opt})} = E^{\mathrm{low}}_{(\mathrm{Ice,opt})} - \left[E^{\mathrm{low}}_{(\mathrm{ice\ model})} + E^{\mathrm{high}}_{(\mathrm{ice\ model})}\right], \quad (3)$$

$$E_{(\mathrm{Bz,opt})} = E^{\mathrm{high}}_{(\mathrm{Bz,opt}),} \quad (4)$$

where the level of theory denoted by 'low' is PBE-D3/MOLOPT-TZV2P and the level of theory denoted by 'high' is DLPNO-CCSD(T)/CBS. Note that to compute the latter, we use the EC extrapolation approach of Jurečka et al. (2006) along with the aug-ano-pVnZ basis sets (see more details in Section 3). The overall benzene–ice system is split into a region of interest (the model system) and the rest of the system (see also Fig. 1 for a visual representation of the ONIOM decomposition used). The model system in equation (2) is defined as the benzene molecule and all complete water molecules within 5 Å of its centre of mass. Those same ice molecules also make up the 'ice model' system in equation (3), but this time with the relaxed geometry they adopt in a fully optimized ice surface. Finally, the last component of the interaction energy (equation 4) is simply obtained from a DLPNO-CCSD(T)/CBS calculation for the fully optimized geometry of benzene at the PBE-D3/MOLOPT-TZV2P level of theory.

We also include zero-point energy (ZPE) corrections using the harmonic frequencies computed at the PBE-D3/MOLOPT-TZV2P (low level) for all three components of equation (1). Each of these corrections are then scaled using a factor of 1.0160 recommended by Kesharwani, Brauer & Martin (2015) to account for anharmonicities in ZPE calculations (note that value was originally derived for PBE/def2-TZVPP calculations).

3 COMPUTATIONAL DETAILS

3.1 Ice XIh model

As in our previous study (see Clark & Benoit (2021) for more details), we use an ice surface obtained at the PW91/PW(350 Ry cut-off) level of theory by Hirsch & Ojamäe (2004), which is repeated to create a $6 \times 3 \times 2$ supercell. Our final model contains 36 unit cells of XIh ice in the slab, 288 H_2O molecules, with four double layers of water molecules. The surface is chosen along the c direction with an increased lattice constant ($c = 34.6716$ Å) to accommodate the adsorption of a benzene molecule. The surface is relaxed such that the topmost water double layer (72 H_2O molecules) is optimized, while the coordinates of the bottom three double layers (216 H_2O molecules) of ice remains fixed. We use surface periodic boundary conditions in the x, y (a, b) directions, while the z (c) direction is treated non-periodically.

3.2 DFT calculations

All PBE-D3 calculations were performed using the Gaussian plane wave (GPW) method implemented in the QUICKSTEP module (Goedecker, Teter & Hutter 1996; Perdew, Burke & Ernzerhof 1996; VandeVondele et al. 2005) of CP2K (v4.1 and v6.1) (Naumkin & Knowles 1995; Chergui 1996; Goedecker et al. 1996; Lippert, Hutter & Parrinello 1997; VandeVondele & Hutter 2007). The valence electrons are described using a TZV2P-MOLOPT-GTH basis set (Dunning 1971; Krack 2005; VandeVondele & Hutter 2007), along with an auxiliary plane-wave cut-off of 300 Ry. The MOLOPT basis set family is optimized to reduce basis-set superposition error (BSSE) in periodic calculations (see VandeVondele & Hutter (2007)), as this can often be an issue for binding energy calculations, and has been shown to be roughly equivalent to a standard quadruple-zeta basis in terms of BSSE error. The core electrons are represented using Goedecker–Teter–Hutter (GTH) pseudo potentials (Krack 2005).

XY periodicity was used for all calculations combined with an analytical Poisson solver for the electrostatic energy. The wave function convergence was set to 1.E−7 a.u.[1] for all calculations. We use identical geometry convergence criteria to Clark & Benoit (2021). The exchange-correlation functional is that derived by Perdew, Burke, and Ernzerhof (PBE) (Perdew et al. 1996) and we account for dispersion interactions using the DFT-D3 correction scheme of Grimme et al. (2010) based on a damped atom-pairwise potential and three-body C_9 corrections (ATM correction; Moellmann & Grimme 2014). Note that the DFT-D3 methodology was parametrized for basis sets of quadruple-zeta quality, assuming that those are near the basis-set limit (Grimme et al. 2010). The geometry of the adsorbed benzene on ice, along with selected structural parameters have been reported in Clark & Benoit (2019) and a coordinate file was provided in the SI of Clark & Benoit (2021).

3.3 DLPNO-CCSD(T)/EC2-CBS calculations

The complete basis set extrapolation of the domain-based local-pair natural orbital coupled-cluster singles doubles and perturbative triples [DLPNO-CCSD(T)] energy was performed using the ORCA 3.0.3 suite of programmes. Note that this particular version of ORCA, the (T) implementation uses a 'semi-canonical' approximation to compute the perturbative triples correction, also known as T0 correction. The expression used for the EC2-CBS extrapolation, due to Jurečka et al. (2006) is

$$\begin{aligned} &E(\mathrm{DLPNO\text{-}CCSD(T)/EC2\text{-}CBS(X,Y)}) \\ &\quad \approx E(\mathrm{SCF;Y}) + E(\mathrm{DLPNO-CCSD(T);X}) + E(\mathrm{MP2;}\infty) \\ &\quad -E(\mathrm{MP2;X}), \end{aligned} \quad (5)$$

where X and Y are the cardinal number of each basis set used. For our binding energy calculations, we used the aug-ano-pVDZ basis set together with the aug-ano-pVTZ basis set, and thus $X = 2$ and $Y = 3$, respectively. We also compared to a higher level aug-ano-pVTZ and aug-ano-pVQZ basis set combination ($X = 3$ and $Y = 4$) and a near-complete basis approach with the aug-ano-pVQZ and aug-ano-pV5Z basis set combination ($X = 4$ and $Y = 5$).

The MP2 energy is extrapolated using

$$E(\mathrm{MP2;}\infty) = \frac{\mathrm{X}^{\beta} \cdot E(\mathrm{MP2,X}) - \mathrm{Y}^{\beta} \cdot E(\mathrm{MP2,Y})}{\mathrm{X}^{\beta} - \mathrm{Y}^{\beta}}, \quad (6)$$

[1]Note that here 'a.u.' refers to atomic units, while later on 'au' means astronomical units.

Table 1. Computed and measured binding energies for benzene–H_2O and the water dimer. Values are given in kJ mol^{-1} with uncertainties if available. Brackets indicate 'tightPNO' values. All calculations use the cluster geometries from the S22 data base (obtained from www.begdb.com; Řezáč et al. 2008).

System	Method	Binding energy (kJ mol^{-1})
Benzene–H_2O cluster		
	PBE-D3/MOLOPT-TZV2P	−15.08
	DLPNO-CCSD(T)/EC2-CBS(2, 3)	−13.52 (−13.44)
	DLPNO-CCSD(T)/EC2-CBS(3, 4)	−13.29 (−12.85)
	DLPNO-CCSD(T)/EC2-CBS(4, 5)	−13.66 (−13.08)
	CCSD(T)/CBS[a]	−13.77
	Experimental data	
	D_0 (Gotch & Zwier 1992)	$-6.82 \leq D_0 \leq -11.63$
	D_0 (Cheng, Grover & Walters 1995)	-9.4 ± 1.2
	D_0 (Courty et al. 1998)	-10.2 ± 0.4
	Estimated[b] D_e	-13.1 ± 0.4
H_2O–H_2O cluster		
	PBE-D3/MOLOPT-TZV2P	−23.33
	DLPNO-CCSD(T)/EC2-CBS(2, 3)	−20.35 (−20.57)
	DLPNO-CCSD(T)/EC2-CBS(3, 4)	−20.17 (−20.58)
	DLPNO-CCSD(T)/EC2-CBS(4, 5)	−20.36 (−20.63)
	CCSD(T)/CBS[a]	−21.21
	Experimental data	
	D_0 (Rocher-Casterline et al. 2011)	-13.20 ± 0.05
	Estimated[c] D_e	-20.80 ± 0.06

[a]Revised value from Takatani et al. (2010).
[b]Value estimated from the experimental D_0 measurements for benzene–H_2O and benzene–D_2O from Courty et al. (1998) and the zero-point energy values computed for the same systems using rigid-body diffusion Monte Carlo calculations by Benoit & Clary (2000).
[c]Value estimated from the experimental D_0 measurements for the dissociation energy of the water dimer from Rocher-Casterline et al. (2011) and the zero-point energy values computed by Shank et al. (2009).

where $\beta = 2.41$, value optimized by Neese, Hansen & Liakos (2009) and Neese & Valeev (2011).

In order to accelerate the calculations, we used both the RI-JK approximation (Weigend 2008) (with a cc-pVQZ/JK auxiliary basis set, Dunning 1989) and the RI-MP2 approach (Weigend & Häser 1997) (with a aug-cc-pVQZ/C auxiliary basis set, Kendall, Dunning & Harrison 1992). All calculations used the verytightscf convergence criterion of ORCA (Neese 2012). All DLPNO-CCSD(T) calculations used the default ORCA criteria for the PNO generation (NormalPNO) unless stated.

4 RESULTS AND DISCUSSION

4.1 Binding energy

The highly dipolar surface arrangement chosen for the ice surface provides a best-case scenario model for the binding of benzene to an ice surface since it maximizes the number of possible hydrogen-bond donors at the surface. It is expected that a realistic non proton-ordered ice surface (Ih or ASW, for example) would have fewer binding sites available for benzene, although an interesting striped proton ordering has been suggested for ice Ih surface (Buch et al. 2008) and dangling OH bonds are a well-characterized feature of ASW (McCoustra & Williams 1996). Therefore, the results obtained for our model can be considered to provide an upper-bound (i.e. most binding) case for the binding energy of benzene on a water ice surface, which is the aim of our study.

4.1.1 Cluster benchmarks

4.1.1.1 Benzene–water

In order to assess the overall accuracy of the hybrid approach proposed in Section 2, we first perform calculations on the benchmark benzene–H_2O system using the geometry reported in the S22 data base initially developed by Jurečka et al. (2006). Our results are summarized in the top panel of Table 1.

We see that, compared to the revised CCSD(T)/CBS reference energy value of Takatani et al. (2010) for benzene–H_2O, PBE-D3 overestimates the binding energy by about 10 per cent. The slight overestimation of binding energy by the D3 correction has already been observed (Reckien, Eggers & Bredow 2014) for benzene adsorption on metal surfaces, for example. Moreover, our chosen basis set is also known to cause some overbinding for ice Ih (see Brandenburg et al. 2019b, footnote 151). However, given the low computational cost of this approach, this result is still very reasonable. Next, we see that the DLPNO-CCSD(T)/EC2-CBS extrapolation approach in its various format (2, 3), (3, 4), or (4, 5) all lead to good agreement with the extrapolated results of Takatani et al. (2010). The ORCA team recommends the usage of a 'TightPNO' (Liakos et al. 2015) criterion when computing interaction energies for weakly bound systems (those values are reported in brackets in our Table 1). We see here that the (2, 3) extrapolation is in surprisingly good agreement with the full CCSD(T)/EC2-CBS data, with a deviation of only 2 per cent, regardless of the PNO criterion. Keeping in mind that our approach relies on an MP2 estimation for the correlation extrapolation, it is very likely that this outcome is the result of fortuitous error cancellation for this combination of basis sets and/or extrapolation parameters. The (3, 4) extrapolation performs slightly worse than (2, 3), but is still only 3 per cent (7 per cent) away from the reference and the (4, 5) extrapolation is a mere 0.7 per cent (5 per cent) above the reference result.

Another comparison point is provided by the work of Brandenburg et al. (2019a) who used quantum diffusion Monte Carlo to determine the binding energy of a water molecule to benzene. They compute a binding energy of -13.1 ± 0.5 kJ mol^{-1} for their '2-leg' configuration, in very good agreement with the values reported in Table 1.

One interesting conclusion from these results is that, for this particular system, the usage of TightPNO increases computational cost with limited accuracy increase and thus the standard criteria appear to provide a better cost/performance balance in our case. Furthermore, the computational cost of the (2, 3) EC extrapolation are much lower than those of the (4, 5) extrapolation but still lead (fortuitously) to results of similar quality. Finally, we also see that a good agreement with the reference BSSE-corrected data can be achieved without any BSSE corrections (see also supplementary information). While this is not likely to be a conclusion of wide-ranging application, since the larger extrapolations and tighter selection criteria are usually more reliable, it does provide a practical solution for the estimation of binding energies beyond the DFT-D3 level for large systems.

A further measure of the accuracy of the computed binding energies is to compare those to the available experimental data, rather than other high-level calculations. The measurement of the binding energy of the benzene–water complex has been performed using a variety of techniques over the years, leading to values ranging from -6.8 to -11.6 kJ mol^{-1}. A selection of these values are reported in the middle of Table 1 under the section '*experimental data*'. The measurement by Courty et al. (1998) is the most accurate to date and also agrees with the error bars and estimations of previous studies. However, the measured experimental values (D_0) cannot be directly compared with the theoretical binding energies (D_e), as the former include the zero-point vibrational energy of the complex. In their study, Courty et al. (1998) used their D_0 measurements along with early rigid-body diffusion Monte Carlo (RB-DMC) calculations by Gregory & Clary (1996) to estimate $-12.89 \leq D_e \leq 14.80$ kJ mol^{-1}. To provide a slightly tighter D_e estimate, we combined the experimental D_0 measurements for benzene–H_2O and benzene–D_2O from Courty et al. (1998) and the zero-point energy (ZPE) values computed for the same systems using improved RB-DMC calculations by Benoit & Clary (2000) on an accurate model potential. This leads to a value of -13.1 ± 0.4 kJ mol^{-1}, in very good agreement with the reference CCSD(T)/CBS data of Takatani et al. (2010), the DMC estimation of Brandenburg et al. (2019a), and our DLPNO-CCSD(T)/EC2-CBS values, given the nature of the ZPE calculations. This suggests that our value (-13.1 ± 0.4 kJ mol^{-1}) is an accurate experimental D_e value for the benzene water cluster.

4.1.1.2 Water dimer In order to explore if our previous conclusions extends to water (and ice), we briefly investigate the binding energy of the water dimer (also from the S22A benchmark set). Our results are summarized in the lower section of Table 1. We observe here again that PBE-D3 overestimates the binding by a similar amount to the benzene–water case (10 per cent). The extrapolated DLPNO-CCSD(T)/EC2-CBS data is also interesting as they further demonstrate a surprisingly good agreement of the (2, 3) extrapolation, within 4 per cent (3 per cent) deviation from the reference value. As was the case earlier, the (3, 4) data are slightly worse than (2, 3) with a deviation of 5 per cent (3 per cent) at a much increased computational time. Finally, the most accurate (4, 5) extrapolation is of similar quality to the previous results obtained with (2, 3) and lead to a deviation of 4 per cent (3 per cent) from the reference value. We note that the change due to the usage of the 'TightPNO' criterion in the DLPNO-CCSD(T) calculation is marginal, although it does seem to compensate for the level of extrapolation with all three scheme leading to a corrected value of -20.6 kJ mol^{-1}.

An appropriate comparison with experimental data also requires the subtraction of the ZPE from the excellent experimental measurements of D_0 from Rocher-Casterline et al. (2011). Here, we use the ZPE estimate computed using diffusion Monte Carlo by Shank et al. (2009) on a highly accurate model potential. We observe that there is good agreement between the estimated 'experimental' D_e and both the reference CCSD(T)/CBS value and our DLPNO-CCSD(T)/EC2-CBS estimations, without any BSSE correction (see also supplementary information).

These benchmark tests provide a suitable validation of our approach and ascertain the accuracy of both PBE-D3 (about 10 per cent overestimation) and the DLPNO-CCSD(T)/CBS(2, 3) approach (about 4 per cent deviation) as a way of systematically computing the binding energy of molecules interacting with water.

4.1.2 Benzene on ferroelectric ice XIh model

Our results are shown in Table 2. We observe, here too, that PBE-D3 seems to overestimate the binding of benzene on ice, if we compare to the values obtained by Sharma et al. (2016) for the their M06-2X DFT model, for example. This is to be expected, based on both cluster energy comparisons described earlier (see Section 4.1.1) and existing literature (Reckien et al. 2014, for example). Our benchmark cluster data reported in Section 4.1.1 suggests that an error on the PBE-D3 values of 10 per cent is appropriate, which accounts for some of the deviation from the values computed by Sharma et al. (2016).

To improve on our PBE-D3 value, while conserving the collective effects of the ice surface model, we use the method described in Section 2 and obtain values that are in good agreement with those of Sharma et al. (2016) for a similar model (also using a hybrid model, but not including periodicity effects explicitly). Our benchmark cluster data reported in Section 4.1.1 indicates that an error of 4 per cent is appropriate for our approach, leading to a binding energy estimate of $D_e = -36 \pm 1$ kJ mol^{-1}.

Our value is slightly higher (i.e. less negative) than the results reported by Sharma et al. (2016) both for their DFT-based approaches (M06-2X with or without hybrid corrections) and their CCSD-based hybrid estimate. To explain some of this discrepancy, we note that Mackie & DiLabio (2010) have shown that M06-2X can overestimate the binding energy for the benzene-water system, despite M06-2X being overall an accurate functional for weak interactions (Mardirossian & Head-Gordon 2017). Sharma et al. (2016) show a good agreement between M06-2X and DLPNO-CCSD binding energies for their models, but a detailed study by Crittenden (2009) showed that neglecting (T) correction usually lead to underbinding at the basis-set limit. For triple-zeta basis sets, without any basis correction, even CCSD(T) is shown to overestimate the binding energy of benzene water (Feller 1999). To gain further insights into the accuracy of the two approaches, we used M06-2X/6-31+ + G(d,p) and DLPNO-CCSD/cc-pVTZ to compute the binding energy of the benzene–water benchmark system described in Section 4.1.1. Our results showed that both method likely overestimate the binding energy (by 18 per cent for M06-2X, with -16.9 kJ mol^{-1}, and by 10 per cent for DLPNO-CCSD, with -15.1 kJ mol^{-1}). Finally, we also investigated the impact of BSSE on the computed binding energy for benzene on ice XIh and found it to be negligible within the uncertainty of our approach ($\ll 1$ kJ mol^{-1}, see supplementary information). Thus we conclude that our binding energy estimate

Table 2. Computed and measured binding energies for benzene adsorbed on a ferroelectric proton-ordered hexagonal crystalline water ice (XIh) surface. Values are given in kJ mol^{-1} with uncertainties if available. [a] Sharma et al. (2016) reported for the geometry closest to our XIh surface model and their largest quantum subsystem (structure A1 in their study). [b] Estimated zero-point energy correction based on scaled harmonic frequency calculations, details given in the text.

System	Method	Binding energy (kJ mol^{-1})
Benzene–ice (XIh)		
	PBE-D3/MOLOPT-TZV2P	-49 ± 5
	DLPNO-CCSD(T)-hybrid/CBS(2, 3)	-36 ± 1
	DLPNO-CCSD/cc-pVTZ:FF[a]	−43.4
	M06-2X/6-31+ + G(d,p):FF	−43.4
	M06-2X/6-31+ + G(d,p)[a]	−41.5
Suggested D_0	DLPNO-CCSD(T)-hybrid/CBS(2, 3) + ZPE[b]	-34 ± 1
	Experimental data	
	UMIST database Rate12	−63.2
	Thrower et al. (2009) (TPD@ASW)	-41.0 ± 0.5
	Stubbing (2019) (TPD@ASW)	-42 ± 6
	Stubbing (2019) (TPD@CI)	-39 ± 3

is more representative of the benzene binding energy to crystalline water ice (XIh).

In order to be able to compare with experimental data, we also need to include zero-point energy (ZPE) correction for this system. This is somewhat more problematic as a full optimization of the benzene + ice system is not an easy task. Here, we explore two ways of doing this. First, the simplest approach is to only consider the translation and rotation (TR) modes of benzene on ice and use those to compute the ZPE. Those modes are traditionally removed through projection in most codes, but can easily be extracted from the unpurified Hessian matrix. The difference between the harmonic TR modes for benzene ice and benzene gives us a ZPE of 154 cm^{-1} (1.85 kJ mol^{-1}). In order to account for anharmonicty, we use here the scaling approach of Kesharwani et al. (2015) and use a scaling factor of 1.016 for PBE, leading to a 'corrected' ZPE of 157 cm^{-1} (1.88 kJ mol^{-1}). An alternative approach is to consider both the benzene and the first ice layer, directly in contact with the adsorbate. This option is computationally more expensive and requires careful control over the optimization of the equilibrium geometry for both benzene on ice and for the isolated ice model. After frequency projection (in this case, the overall translations and rotations modes are not relevant for intermolecular ZPE), we obtain a ZPE of 161 cm^{-1} (1.93 kJ mol^{-1}), in very close agreement with our earlier simpler approach. The anharmonic value obtained using the PBE scaling factor of 1.016 defined above leads to a 'corrected' ZPE of 164 cm^{-1} (1.96 kJ mol^{-1}).

The work from Slipchenko & Gordon (2008) shows a similar trend in their ZPE corrections, where their benzene–water binding energy is only increased by about 1 kcal mol^{-1} (4.2 kJ mol^{-1}) from their computed D_e value. Feller (1999) also suggests a similar value of 1 kcal mol^{-1} (4.2 kJ mol^{-1}) value for the ZPE correction of the same complex. If we account for anharmonic corrections and keep in mind that the values reported in both studies are for a *single* water molecule binding to a benzene molecule, those estimations broadly agree with ours. Indeed, the lower mobility of the water molecules in the ice lattice is likely causing the low impact of benzene on the benzene–ice ZPE correction.

Our estimate for the experimental binding energy is thus $D_0 = -34 \pm 1$ kJ mol^{-1}, which is nearly half the value of the Rate12 UMIST database commonly used in astrochemical modelling (see also Table 2). This new estimate is in good agreement with the TPD measurements of Thrower et al. (2009) (-41.0 ± 0.5 kJ mol^{-1}, recommended average value from their desorption study) and Stubbing & Brown (Stubbing 2019) for benzene on ASW (-42 ± 6 kJ mol^{-1}). We also note that the binding energy obtained from TPD of benzene on crystalline ice (CI) leads to a slightly lower value of -39 ± 3 kJ mol^{-1} (Stubbing 2019), also in close agreement with our estimate. This implies either that the simple ordered model we developed gives a realistic description of the local environment experienced by benzene on ASW (i.e. on a local scale, the binding mode of benzene in ASW resembles that of ice XIh), or that the uncertainly in both experiments or our calculations is still too large to be able to differentiate between the two types of ices (crystalline XIh and amorphous ASW). We are currently exploring this avenue further and will report our findings in a future publication.

4.2 Astrophysical implications

To test the impact of the binding energy for benzene calculated here (-34 kJ mol^{-1} or a desorption energy of 4090 K), we adopt this value in a chemical model of a carbon-rich AGB outflow (Van de Sande, Walsh & Millar 2021) and the mid-plane of a protoplanetary disc around a T Tauri star (Walsh, Nomura & van Dishoeck 2015). We compare the results with the value listed in the Rate12 version of the UMIST Database for Astrochemistry (UDfA, 7587 K; McElroy et al. 2013). Full details of both models are given in the provided references and we provide here some brief details only. Both models use the full UDfA gas-phase chemical network supplemented with gas–grain interactions (including accretion, thermal desorption, and non-thermal desorption driven by stellar and interstellar photons and cosmic ray induced photons, and reactive desorption) and a sub-set of the grain-surface network (and associated gas-phase chemistry and gas–grain interactions) from Garrod, Widicus Weaver & Herbst (2008). The AGB outflow model also includes sputtering from grains as a desorption mechanism (see Van de Sande et al. 2019, for further details).

4.2.1 *Carbon-rich AGB outflow*

The AGB outflow model adopts parameters similar to the well-studied carbon-rich AGB star, IRC + 10216: a mass-loss rate of 10^{-5} M$_\odot$ yr^{-1}, a constant outflow velocity of 15 km s^{-1}, a stellar temperature of 2000 K, and a temperature profile characterized by a power law with exponent 0.7 (Van de Sande et al. 2021). We run four

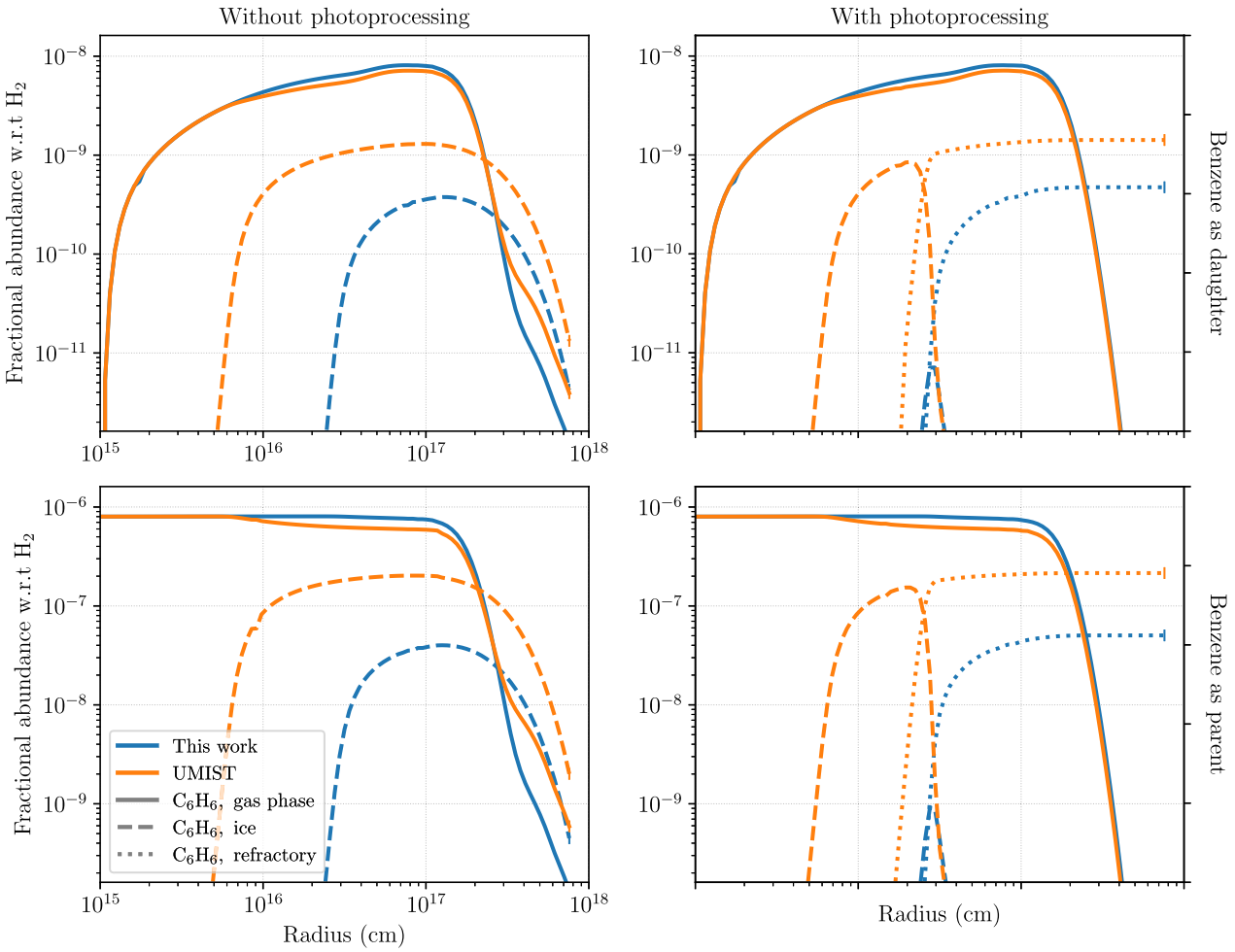

Figure 2. Fractional abundance (with respect to H_2) for gas-phase benzene (solid lines), ice-phase benzene (dashed lines) and 'refractory phase' benzene (dotted lines) for models in which benzene is assumed to be a daughter species (top row) and in which benzene is assumed to be a parent species (bottom row), and for models excluding (left) and including (right) the photoprocessing of carbon-rich ices to refractory organics. The results when adopting the UDfA value of the benzene binding energy (7587 K) are given in orange, and those using the binding energy calculated in this work (4090 K) are given in blue.

variations of the outflow model; one in which we assume that benzene is a daughter species only (with a zero initial abundance), and one in which benzene is assumed to be formed in the inner wind and is thus a parent species. The parents species and abundances are those of Agúndez, Cernicharo & Guélin (2010). The initial abundance of benzene when included as a parent species is 8.7×10^{-7} with respect to H_2, or two orders of magnitude less than the abundance of the parent C_2H_2, which is consistent with the model predictions of inner wind chemistry from Cherchneff (2012). Note that gas-phase benzene is yet to be detected in the outflow of an AGB star; hence, we use an optimistic value from the models for this case. For each set of initial abundances, we also run a version of the model in which we include gas-phase and gas–grain chemistry only (as done in Van de Sande et al. 2019), and one in which we also enable the processing of carbon-chain species to form refractory organics (as described in Van de Sande et al. 2021).

Fig. 2 shows the fractional abundance of benzene with respect to H_2 in the gas phase (solid lines) and ice phase (dashed lines) for the models in which benzene is a daughter species (top row) and in which benzene is a parent species (bottom row). The left-hand and right-hand plots show the model results excluding and including, respectively, the photo-processing of carbon-rich ices to form refractory organics. In the right-hand plots, the fractional abundance of benzene 'converted' to refractory form is shown by the dotted lines. The results from the models that adopt the default UDfA value are shown in orange, and the model using the binding energy from this work are shown in blue.

The models in which benzene is assumed to be a parent predict a much larger peak fractional abundance of gas-phase benzene in the outflow ($\sim 10^{-6}$ versus $\sim 10^{-8}$ with respect to H_2). The models show that if benzene is a parent species, it is able to persist in the gas phase at (close to) the assumed initial abundance until a radius of $\approx 2 \times 10^{17}$ cm at which point it starts to be dissociated by interstellar UV photons. In the models in which benzene is a daughter species, the fraction abundance peaks at a radius of $\sim 10^{17}$ cm. The formation of gas-phase benzene in this case is via ion–molecule chemistry. C_6H_6 is produced by dissociative recombination with electrons by $C_6H_7^+$, which is formed by radiative association of H_2 with $C_6H_5^+$. $C_6H_5^+$ formation is linked to the protonation of C_2H_2 to $C_2H_3^+$, which then reacts with C_2H_2 to form $C_4H_3^+$ and subsequently $C_6H_5^+$.

In the models without photoprocessing, the use of the lower binding energy has a negligible effect on the peak abundance and

column density of gas-phase benzene both in the models in which it is a daughter species and in the models in which it is a parent species. However, the peak fractional abundance of ice-phase benzene (i.e. benzene that is bound to the ice) drops by a factor of ≈ 2 for the model in which benzene is a daughter, and by a factor of ≈ 4 in the model in which benzene is a parent.

In the models with photoprocessing, gas-phase benzene is similarly unaffected by the change in binding energy. The model adopting the lower binding energy predicts a lower peak fractional abundance of 'refractory' benzene by a factor of ≈ 3 for the case where benzene is a daughter, and by a factor of ≈ 4 for the case where benzene is a parent. The use of the lower binding energy also delays the onset of freezeout (and thus conversion to 'refractory' benzene) from a radius of $\approx 5 \times 10^{15}$ cm to a radius of ≈ 2–3×10^{16} cm. The lower binding energy for this model predicts significantly less benzene in the ice phase than that using the higher binding energy.

To summarize, the impact of using a lower binding energy for benzene has negligible impact on the gas-phase benzene through the outflow, but lowers both the ice-phase and refractory-phase benzene. The model including the photoprocessing of ices and the lower binding energy calculated here predicts negligible amounts of benzene in the ice phase.

4.2.2 *Disc mid-plane of a T Tauri star*

The protoplanetary disc model is the T Tauri disc model described in Walsh et al. (2015). Because we are modelling the chemical structure of the warm and dense inner disc mid-plane that is well shielded from radiation, we include only gas-phase chemistry and gas–grain interactions (accretion, and thermal and non-thermal desorption driven by cosmic rays); that is, we do not include grain-surface reactions nor reactive desorption. The initial abundances adopted in this model are taken from a dark cloud chemical model with a temperature of 10 K, a number density of 10^4 cm^{-3}, and a cosmic ray ionization rate of 1.3×10^{-17} s^{-1}. Abundances are extracted at a time of 3×10^5 yr. Note that the binding energy adopted for benzene in the dark cloud model is the default value from UdFA (7587 K). The initial abundance of benzene in this model is 2.6×10^{-11} in the gas phase and 6.5×10^{-12} in the ice phase, with respect to total H nuclei density.

The left-hand panel of Fig. 3 shows the temperature profile for the disc model from Walsh et al. (2015). The temperature decreases as a function of radius from a value of 265 K at 1 au to a value of 85 K at 4 au. Note that this disc has two sources of heating in the inner mid-plane: passive heating from the central star and heating from accretion (see Nomura et al. 2007, for more details on the physical model of the disc).

The right-hand panel of Fig. 3 shows the fractional abundance of gas-phase and ice-phase benzene as function of radius. For the default UDfA value for the benzene binding energy, the benzene snowline lies at $\approx$1.8 au. When adopting the value calculated here, the benzene snowline shifts outwards to $\approx$22 au. Note that the apparent gap in the amount of benzene in the disc for the model adopting the UDfA value is an artefact of plotting the abundances on a log scale. The abundance of gas-phase benzene in this model drops quickly to negligible values, whereas the abundance of ice-phase benzene rises quickly from a negligible value in the inner disc. Hence, the model adopting the binding energy calculated in this work predicts a larger and more radially extended reservoir of gas-phase benzene in the inner disc. This is a similar trend to that found by Woods & Willacy (2007) who also explored the impact of benzene binding energy on the distribution and abundance of benzene in the inner disc, albeit for a different disc model and network than that used here. Woods & Willacy (2007) saw the benzene snowline move from $\approx$1 to $\approx$2 au when decreasing the binding energy of benzene from 7587 to 4750 K. This lower value comes from estimates of the heats of adsorption of benzene to a graphite surface using gas–solid chromatography (Arnett, Hutchinson & Healy 1988), and is very close to the value calculated here. Also evident in these results is the efficient formation of gas-phase benzene in the inner disc, increasing from an initial fractional abundance of 2.6×10^{-11} to a value of $\approx 2 \times 10^{-8}$ with respect to total H nuclei density (note that in the inner disc, most of the hydrogen is in molecular form). This boost in the abundance of gas-phase benzene is due to efficient ion–molecule chemistry: C_6H_6 is formed via the recombination of $C_6H_7^+$ with negatively charged grains that are the main charge carriers in this region of the disc, being some two to three orders of magnitude more abundant than electrons. $C_6H_7^+$ formation, in turn, is dominated by the barrierless reaction between $C_3H_4^+$ and CH_3CCH with the former produced predominantly by cosmic-ray-induced photoionization of CH_3CCH and the latter from the recombination of $C_4H_5^+$ with negatively charged grains. This mechanism of benzene formation in the inner disc is also described in Woods & Willacy (2007).

5 CONCLUSION

In this paper, we have presented a reliable upper bound (i.e. largest) value for the binding energy of benzene on an ordered water ice surface (-34 kJ mol^{-1} or a desorption energy of 4090 K, when including zero-point energy corrections). Our estimation is based on a carefully calibrated hybrid method that includes both a high-level treatment of electronic correlation, through the DLPNO-CCSD(T) approach, and the influence of surface periodicity through GPW DFT. We have shown that our benzene–ice binding energy is different from what has been used in astrochemical models, sometimes by up to 50 per cent. We also compared our estimations with TPD data. While two sets of experiments are performed on amorphous structured water (ASW) ice and one on crystalline water ice, we find that all three values agree well with our computed highly ordered crystalline ice data. This implies that our simple ordered model describes realistically the local environment experienced by benzene on ASW (i.e. on a local scale, the binding mode of benzene in ASW resembles that of ice XIh).

We also explored the influence of this revised binding energy on astrophysical models. Inputting our value into a model of the gas–grain chemistry occurring in an AGB outflow shows that using the lower value delays the onset of freezeout (and thus depletion) of benzene in the wind. When photoprocessing is included, the lower binding energy has the additional effect of limiting the abundance benzene in the ice phase to negligible values. The new binding energy also predicts a shift outwards in the position of the benzene snowline in the mid-plane of a protoplanetary disc by $\approx$0.4 au (this work) to $\approx$1 au (Woods & Willacy 2007). Hence, a lower binding energy predicts a larger reservoir of gas-phase benzene in the inner disc compared with the default UDfA value. We note here that gas-phase benzene has been detected in now two protoplanetary discs for the first time with *JWST* (Tabone et al. 2023; Arabhavi et al. 2024). The impact of this lower binding energy on the abundance and distribution of gas-phase benzene in the inner disc should be explored in future work, especially under carbon-rich conditions, given this new result from *JWST*. Based on our work, we recommend using this revised value (-34 kJ mol^{-1} or a desorption energy of 4090 K) for the binding energy of benzene on water ice in astrochemical models.

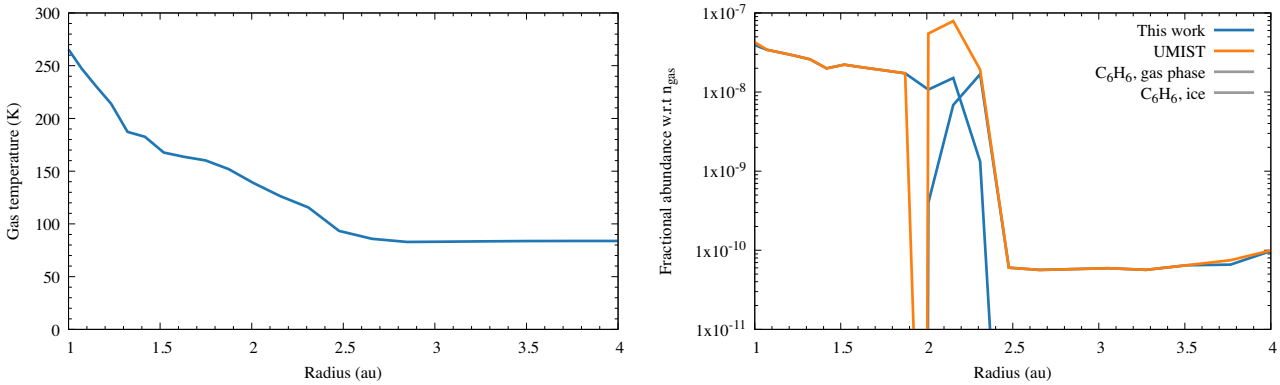

Figure 3. Temperature profile (right) of the inner mid-plane for a disc around a T Tauri star (from the models presented in Walsh et al. 2015). Fractional abundance (with respect to total gas density) for gas-phase benzene (solid lines) and ice-phase benzene (dashed lines) for a model in which the binding energy from this work was adopted (4090 K; blue) and for a model using the default UDfA value (7587 K; orange).

ACKNOWLEDGEMENTS

We thank Dr James Stubbing and Professor Wendy Brown (University of Sussex, UK) for generously providing experimental data used in this work. We also thank Dr Gerrit Brandenburg for helpful comments and suggestions regarding the binding energy computation. We acknowledge the Viper High Performance Computing facility of the University of Hull and its support team. DMB acknowledges financial support from the Science and Technology Facilities Council (grant number ST/R000840/1). MVdS acknowledges support from the European Union's Horizon 2020 research and innovation programme under the Marie Sklodowska-Curie grant agreement no. 882991 and the Oort Fellowship at Leiden Observatory. CW acknowledges financial support from the University of Leeds, the Science and Technology Facilities Council, and UK Research and Innovation (grant numbers ST/X001016/1 and MR/T040726/1).

DATA AVAILABILITY

All data used for this study are provided in this paper or references herein.

REFERENCES

Agúndez M., Cernicharo J., Guélin M., 2010, ApJ, 724, L133
Arabhavi A. M. et al., 2024, Science, 384, 1086
Arnett E. M., Hutchinson B. J., Healy M. H., 1988, J. Am. Chem. Soc., 110, 5255
Benoit D. M., Clary D. C., 2000, J. Chem. Phys., 113, 5193
Benoit D. M., Chavagnac A. X., Clary D. C., 1998, Chem. Phys. Lett., 283, 269
Bovolenta G. M., Vogt-Geisse S., Bovino S., Grassi T., 2022, ApJS, 262, 17
Brandenburg J. G. et al., 2019a, J. Phys. Chem. Lett., 10, 358
Brandenburg J. G., Zen A., Alfè D., Michaelides A., 2019b, J. Chem. Phys., 151, 164702
Buch V., Groenzin H., Li I., Shultz M., Tosatti E., 2008, Proc. Natl. Acad. Sci. USA, 105, 5969
Burkhardt A. M., Loomis R. A., Shingledecker C. N., Lee K. L. K., Remijan A. J., McCarthy M. C., McGuire B. A., 2021, Nat. Astron., 5, 181
Cernicharo J., Heras A. M., Tielens A. G. G. M., Pardo J. R., Herpin F., Guélin M., Waters L. B. F. M., 2001, ApJ, 546, L123
Cheng B.-M., Grover J., Walters E., 1995, Chem. Phys. Lett., 232, 364
Cherchneff I., 2012, A&A, 545, A12
Chergui M., 1996, Femtochemistry: Ultrafast Chemical and Physical Processes in Molecular Systems. Singapore, World Scientific
Clark V. H., Benoit D. M., 2019, Int. Astron. Un. Proc. Int. Astron. Un., 15, 468
Clark V. H., Benoit D. M., 2021, MNRAS, 508, 3239
Cooke I. R., Gupta D., Messinger J. P., Sims I. R., 2020, ApJ, 891, L41
Courty A., Mons M., Dimicoli I., Piuzzi F., Gaigeot M.-P., Brenner V., de Pujo P., Millié P., 1998, J. Phys. Chem. A, 102, 6590
Crittenden D. L., 2009, J. Phys. Chem. A, 113, 1663
Dapprich S., Komàromi I., Byun K., Morokuma K., Frisch M. J., 1999, J. Mol. Struct., 461–462, 1
Delsemme A., 1975, Icarus, 24, 95
Dunning T. H., 1971, J. Chem. Phys., 55, 716
Dunning T. H., 1989, J. Chem. Phys., 90, 1007
Engdahl A., Nelander B., 1985, J. Phys. Chem., 89, 2860
Feller D., 1999, J. Phys. Chem. A, 103, 7558
Ferrero S., Zamirri L., Ceccarelli C., Witzel A., Rimola A., Ugliengo P., 2020, ApJ, 904, 11
Garrod R. T., Herbst E., 2006, A&A, 457, 927
Garrod R. T., Widicus Weaver S. L., Herbst E., 2008, ApJ, 682, 283
Goedecker S., Teter M., Hutter J., 1996, Phys. Rev. B, 54, 1703
Gotch A. J., Zwier T. S., 1992, J. Chem. Phys., 96, 3388
Gregory J. K., Clary D. C., 1996, Mol. Phys., 88, 33
Grimme S., Antony J., Ehrlich S., Krieg H., 2010, J. Chem. Phys., 132, 154104
Hirsch T. K., Ojamäe L., 2004, J. Phys. Chem. B, 108, 15856
Jones B. M., Zhang F., Kaiser R. I., Jamal A., Mebel A. M., Cordiner M. A., Charnley S. B., 2011, Proc. Natl. Acad. Sci. USA, 108, 452
Jurečka P., Šponer J., Černý J., Hobza P., 2006, Phys. Chem. Chem. Phys., 8, 1985
Kendall R. A., Dunning T. H., Harrison R. J., 1992, J. Chem. Phys., 96, 6796
Kesharwani M. K., Brauer B., Martin J. M. L., 2015, J. Phys. Chem. A, 119, 1701
Koskinen T. T., Moses J. I., West R. A., Guerlet S., Jouchoux A., 2016, Geophys. Res. Lett., 43, 7895
Krack M., 2005, Theor. Chem. Acc., 114, 145
Kraemer K. E., Sloan G. C., Bernard-Salas J., Price S. D., Egan M. P., Wood P. R., 2006, ApJ, 652, L25
Liakos D. G., Sparta M., Kesharwani M. K., Martin J. M. L., Neese F., 2015, J. Chem. Theory Comput., 11, 1525
Lippert G., Hutter J., Parrinello M., 1997, Mol. Phys., 92, 477
Mackie I. D., DiLabio G. A., 2010, Phys. Chem. Chem. Phys., 12, 6092
Malek S. E., Cami J., Bernard-Salas J., 2012, ApJ, 744, 16
Mardirossian N., Head-Gordon M., 2017, Mol. Phys., 115, 2315
McCoustra M., Williams D. A., 1996, MNRAS, 279, L53
McElroy D., Walsh C., Markwick A. J., Cordiner M. A., Smith K., Millar T. J., 2013, A&A, 550, A36
McGuire B. A., Burkhardt A. M., Kalenskii S., Shingledecker C. N., Remijan A. J., Herbst E., McCarthy M. C., 2018, Science, 359, 202

Moellmann J., Grimme S., 2014, J. Phys. Chem. C, 118, 7615
Naumkin F. Y., Knowles P. J., 1995, J. Chem. Phys., 103, 3392
Neese F., 2012, WIREs Comput. Mol. Sci., 2, 73
Neese F., Valeev E. F., 2011, J. Chem. Theory Comput., 7, 33
Neese F., Hansen A., Liakos D. G., 2009, J. Chem. Phys., 131, 064103
Nomura H., Aikawa Y., Tsujimoto M., Nakagawa Y., Millar T. J., 2007, ApJ, 661, 334
Perdew J. P., Burke K., Ernzerhof M., 1996, Phys. Rev. Lett., 77, 3865
Reckien W., Eggers M., Bredow T., 2014, Beilstein J. Org. Chem., 10, 1775
Řezáč J. et al., 2008, Collect. Czechoslov. Chem. Commun., 73, 1261
Rocher-Casterline B. E., Ch'ng L. C., Mollner A. K., Reisler H., 2011, J. Chem. Phys., 134, 211101
Schuhmann M. et al., 2019, A&A, 630, A31
Shank A., Wang Y., Kaledin A., Braams B. J., Bowman J. M., 2009, J. Chem. Phys., 130, 144314
Sharma D., Sameera W., Andersson S., Nyman G., Paterson M. J., 2016, Comput. Phys. Commun. 17 4079
Silva S. C., Devlin J. P., 1994, J. Phys. Chem., 98, 10847
Slipchenko L. V., Gordon M. S., 2008, J. Phys. Chem. A, 113, 2092–2102
Stubbing J. W., 2019, PhD thesis, University of Sussex
Suzuki S., Green P. G., Bumgarner R. E., Dasgupta S., Goddard W. A., Blake G. A., 1992, Science, 257, 942
Tabone B. et al., 2023, Nat. Astron., 7, 805
Takatani T., Hohenstein E. G., Malagoli M., Marshall M. S., Sherrill C. D., 2010, J. Chem. Phys., 132, 144104
Thrower J., Collings M., Rutten F., McCoustra M., 2009, J. Chem. Phys., 131, 244711
Tinacci L., Germain A., Pantaleone S., Ferrero S., Ceccarelli C., Ugliengo P., 2022, ACS Earth Space Chem., 6, 1514
Van de Sande M., Walsh C., Mangan T. P., Decin L., 2019, MNRAS, 490, 2023
Van de Sande M., Walsh C., Millar T. J., 2021, MNRAS, 501, 491
VandeVondele J., Hutter J., 2007, J. Chem. Phys., 127, 114105
VandeVondele J., Krack M., Mohamed F., Parrinello M., Chassaing T., Hutter J., 2005, Comput. Phys. Commun., 167, 103
Waite J. H., Young D. T., Cravens T. E., Coates A. J., Crary F. J., Magee B., Westlake J., 2007, Science, 316, 870
Walsh C., Nomura H., van Dishoeck E., 2015, A&A, 582, A88
Weigend F., 2008, J. Comput. Chem., 29, 167
Weigend F., Häser M., 1997, Theor. Chem. Acc., 97, 331
Woods P. M., Willacy K., 2007, ApJ, 655, L49
Zamirri L., Ugliengo P., Ceccarelli C., Rimola A., 2019, ACS Earth Space Chem., 3, 1499

SUPPORTING INFORMATION

Supplementary data are available at *MNRAS* online.

Please note: Oxford University Press is not responsible for the content or functionality of any supporting materials supplied by the authors. Any queries (other than missing material) should be directed to the corresponding author for the article.

This paper has been typeset from a TEX/LATEX file prepared by the author.